The Radical Cation of *anti*-Tricyclooctadiene and Its Rearrangement Products

Thomas Bally,*[a] Stefan Bernhard,[a] Stephan Matzinger,[a] Leo Truttmann,[a] Zhendong Zhu,[a] Jean-Luc Roulin,[a] Andrzej Marcinek,*[b] Jerzy Gebicki,[b] Ffrancon Williams,*[c] Guo-Fei Chen,[c] Heinz D. Roth,[d] and Torsten Herbertz[d]

Abstract: The *anti* dimer of cyclobutadiene (*anti*-tricyclo[4.2.0.0^{2,5}]octa-3,7-diene, **TOD**) is subjected to ionization by γ-irradiation in Freon matrices, pulse radiolysis in hydrocarbon matrices, and photoinduced electron transfer in solution. The resulting species are probed by optical and ESR spectroscopy (solid phase) as well as by CIDNP spectroscopy (solution). Thereby it is found that ionization of *anti*-**TOD** invariably leads to spontaneous decay to two products, that is bicyclo[4.2.0]octa-2,4,7-triene (**BOT**) and 1,4-dihydropentalene (1,4-**DHP**), whose relative yield strongly depends on the conditions of the experiment. Exploration of the $C_8H_8^{\bullet+}$ potential energy surface by the B3LYP/6-31G* density functional method leads to a mechanistic hypothesis for the observed rearrangements which involves a bifurcation between a pathway leading to the simple valence isomer, **BOT**$^{\bullet+}$, and another one leading to an unprecedented other valence isomer, the *anti* form of the bicyclo[3.3.0]octa-2,6-diene-4,8-diyl radical cation (*anti*-**BOD**$^{\bullet+}$). The latter product undergoes a very facile H-shift to yield the radical cation of 1,3a-dihydropentalene (1,3a-**DHP**$^{\bullet+}$) which ultimately rearrranges by a further H-shift to the observed product, 1,4-**DHP**$^{\bullet+}$.

Keywords: electronic structure · radical ions · rearrangements · spectroscopy · theoretical calculations

Introduction

The *syn* and *anti* forms of tricyclo[4.2.0.0^{2,5}]octa-3,7-diene (**TOD**) occupy a central position among the thirteen isomers of the $(CH)_8$ family that have been isolated.[1] Thus, in terms of ring strain, their structures are intermediate between the extremes of cubane and cyclooctatetraene (**COT**). Moreover, in contrast to the more complex skeletal nature of several of the other isomers, the *syn* form of these cyclobutadiene dimers and bicyclo[4.2.0]octa-2,4,7-triene (**BOT**) represent the simplest contiguous $(CH)_8$ species that arise on the reaction pathway from cubane to **COT** through progressive C–C bond scission. Accordingly, as a logical extension of previous work on the radical cation of **COT** and its transformations,[2, 3] the **TOD** isomers were selected for detailed studies. In addition, if the parent radical cations would turn out to be sufficiently stable to be observed in our experiments, we expected to gain some insight into the operation of the transannular through-bond and through-space interactions of the two π-systems in **TOD**.[4]

[a] Prof. T. Bally, Dr. S. Bernhard,[+] Dr. S. Matzinger, Dr. L. Truttmann, Dr. Z. Zhu, J.-L. Roulin
Institut de Chimie Physique, Université de Fribourg, Pérolles
1700 Fribourg (Switzerland)
Fax: (+41) 26-300-9737
E-mail: Thomas.Bally@unifr.ch

[b] Dr. A. Marcinek, Prof. J. Gebicki
Institute of Applied Radiation Chemistry
Technical University of Lodz
90–924 Lodz (Poland)
Fax: (+48) 42-636 5008
E-mail: marcinek@ck-sg.p.lodz.pl

[c] Prof. F. Williams, Dr. G.-F. Chen
Department of Chemistry, University of Tennessee
Knoxville, TN 37996–1600 (USA)
Fax: (+1) 865-974-3454
E-mail: ffwilliams@utk.edu

[d] Prof. H. D. Roth, T. Herbertz
Department of Chemistry, Rutgers University
New Brunswick, NJ 08854-8087 (USA)
Fax: (+1) 732-445-5312
E-mail: roth@rutchem.rutgers.edu

[+] Current address:
Department of Chemistry and Chemical Biology
Cornell University
Ithaca, NY 14853-1301 (USA)

Supporting information for this article is available on the www under http://www.wiley-vch.de/home/chemistry/ or from the author.

  0947-6539/00/0605-0849 $ 17.50+.50/0

Aside from the structural questions, the radical cation reactivity of the two isomers of **TOD** might be expected to differ only slightly, insofar as the radical cations of **BOT** and **COT** would appear to be the most likely rearrangement products in both cases. Our previous work on $(CH)_8$ species[2, 3, 5–7] has shown, however, that radical cation chemistry does not necessarily mimic the reactivity of the neutral molecules, and that unusual rearrangements can occur, especially on photoexcitation. Indeed, we find such a rich diversity in behavior between the chemistry of *syn*- and *anti*-**TOD**$^{\bullet+}$ that the results are largely complementary, with only **BOT**$^{\bullet+}$ featuring as a common rearrangement product from both of these isomeric species (attained, however, via very different pathways).

In this first paper, we present a detailed study of the radical cation species formed as a result of the ionization of the *anti*-**TOD** isomer and its subsequent rearrangements. The predominant primary product of its rearrangement in some crystalline Freon matrices is indeed the **BOT** radical cation, and we have characterized this species definitively by ESR measurements. Further confirmation of its role in the reaction sequence has been obtained from CIDNP and EA studies, and therefore its identity has been established beyond question. This information has in turn been instrumental in establishing the role of **BOT**$^{\bullet+}$ as one of the reaction products in the sequential rearrangements starting from *syn*-**TOD**$^{\bullet+}$, as described in the following paper.

A second significant result of the *anti*-**TOD** ionization experiments reported below is the highly unusual matrix dependence of the yields for the two rearrangement products. In fact, the other main product, 1,4-dihydropentalene radical cation (1,4-**DHP**$^{\bullet+}$), is found to be the dominant one in glassy Freon and hydrocarbon matrices. As will be shown, quantum chemical calculations indicate that the formation of this compound may be attributed to a facile rearrangment of *anti*-**TOD**$^{\bullet+}$ to the *anti* form of bicyclo[3.3.0]octa-2,6-diene-4,8-diyl radical cation (*anti*-**BOD**$^{\bullet+}$) as a fleeting transient on the pathway to 1,4-**DHP**$^{\bullet+}$.

Experimental Results

Radiolytic oxidation of *anti*-TOD in F-112 and F-113: Figure 1 shows the well-resolved ESR spectra a) and b) obtained from the radiolytic oxidation of *anti*-**TOD** in F-113 and F-112, respectively. The spectral patterns are clearly identical except for the slightly improved line definition in b). In order to optimize the resolution without loss of signal intensity, these spectra were recorded just a few degrees below the characteristic transition temperatures of the solid Freons (135–140 K for F-112 and 115 K for F-113). Above these transition points, diffusive motion sets in with radical cation decay and bimolecular ion-molecule reactions resulting in irreversible spectral changes.

The analysis of the multiplet pattern in Figure 1a) and b) was accomplished by means of computer simulation, and an excellent fit (Figure 1c) was achieved using the parameters $a(2\,H) = 25.8$ G, $a(4\,H) = 7.5$ G, and $a(2\,H) = 3.8$ G. The triplet splittings are inconsistent with an assignment of the spectrum

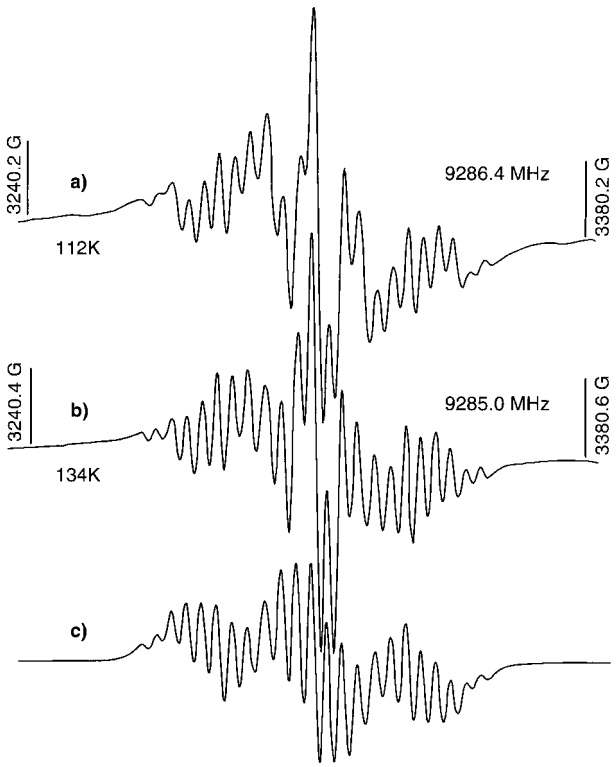

Figure 1. First-derivative ESR spectra obtained from the radiolytic oxidation at 77 K of dilute solutions of *anti*-**TOD** in a) F-113 and b) F-112, and recorded at the stated temperatures to provide optimum resolution in each matrix. The matching spectrum c) was obtained by computer simulation using the following hyperfine coupling parameters: $a(2\,H) = 25.8$ G, $a(4\,H) = 7.5$ G, $a(2\,H) = 3.8$ G, and a linewidth of 2.5 G. These coupling constants agree closely with theoretically calculated values for **BOT**$^{\bullet+}$, and consequently the sharp-line pattern evidenced in spectra a) and b) is assigned to **BOT**$^{\bullet+}$.

to the parent *anti*-**TOD**$^{\bullet+}$ since the pattern should then consist of a quintet of quintets from the two sets of four equivalent hydrogens. Moreover, B3LYP calculations for *anti*-**TOD**$^{\bullet+}$ predict $a(4\,H) = 2.1$ G and $a(4\,H) = -4.2$ G which would correspond to a strikingly different pattern from that observed in Figure 1, as well as a spectral width of only 25 G in comparison with the much larger observed one of 89 G.

On the other hand, both the overall pattern and the magnitudes of the hyperfine couplings are close to those that may be reasonably expected for the radical cation of bicyclo[4.2.0]octa-2,4,7-triene (**BOT**$^{\bullet+}$) with the spin localized in the cyclohexadiene moiety. To account for the observed coupling to four nearly equivalent hydrogens, $a(4\,H) = 7.5$ G, one need only assume that the long-range couplings to the two equivalent olefinic hydrogens at C(7) and C(8) are of similar magnitude (i.e., within the linewidth of 2.5 G) to that for the two equivalent dienic hydrogens at C(2) and C(5). An attractive feature of this assignment to **BOT**$^{\bullet+}$ is that the large triplet splitting $a(2\,H) = 25.8$ G would be expected for the bridgehead β-hydrogens at C(1) and C(6), while the much smaller triplet splitting $a(2\,H) = 3.8$ G is also appropriate for the inner dienic hydrogens at C(3) and C(4).

This assignment is confirned by B3LYP calculations (Table 1) which predict couplings of 24.1 G for the bridgehead, 7.1 G for the olefinic, and -9.0 and -3.2 G for the outer and inner

0947-6539/00/0605-0850 $ 17.50+.50/0 *Chem. Eur. J.* **2000**, *6*, No. 5

dienic hydrogens, respectively. These results are seen to be in excellent accord with the experimental values assigned to the bridgehead and inner dienic hydrogens, while the observed $a(4\,H) = 7.5$ G is also nicely accounted for within the experimental resolution by being intermediate between the respective $a(2\,H)$ couplings of 7.1 and 9.0 G calculated for the olefinic and the outer dienic hydrogens. Thus, there can be little doubt that **BOT**$^{\bullet+}$ is the main signal carrier present after the radiolytic oxidation of *anti*-**TOD** in F-112 and F-113 at 77 K.

ESR evidence for the pathway of **BOT**$^{\bullet+}$ photoconversion to other $C_8H_8^{\bullet+}$ isomers is provided in Figure 2. The spectrum a) resulting from the oxidation of *anti*-**TOD** in F-113 is essentially the same as that already described in Figure 1a), except that the resolution of the dominant **BOT**$^{\bullet+}$ pattern is slightly inferior at 109 K. Illumination with 310–410 nm light (in the 395 nm absorption band of **BOT**$^{\bullet+}$, see below) led to the total loss of the **BOT**$^{\bullet+}$signals and to the growth of a strong central feature, as shown in Figure 2b). The form of this singlet spectrum matches precisely with that of **COT**$^{\bullet+}$ generated from neutral **COT** under the same conditions.

This assignment was in turn confirmed by the clean photoconversion of the singlet to the distinctive spectrum of the *syn*-bicyclo[3.3.0]octa-2,6-diene-4,8-diyl radical cation (*syn*-**BOD**$^{\bullet+}$) with 460–580 nm light, as shown in Figure 2c).

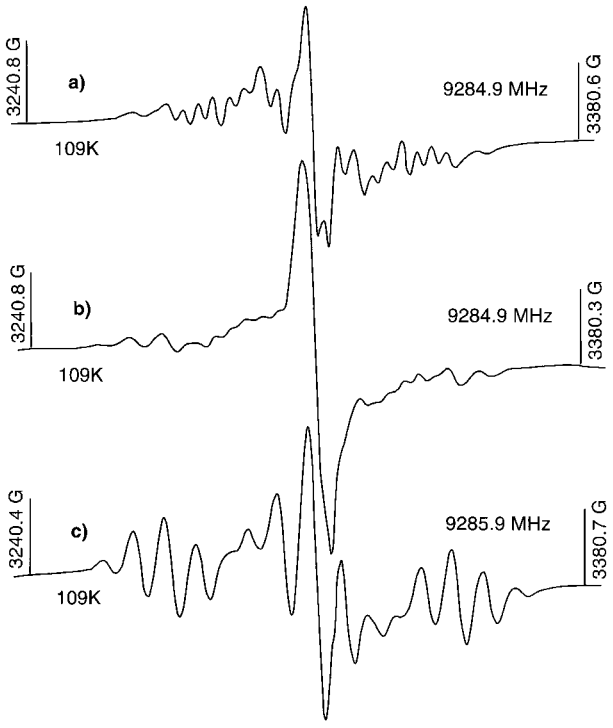

Figure 2. First-derivative ESR spectra showing the stepwise photoconversion of **BOT**$^{\bullet+}$ signals in a) to the strong singlet feature of **COT**$^{\bullet+}$ in b), and subsequently of the latter to the strong well-defined spectrum of **BOD**$^{\bullet+}$ in c). The initial spectrum a) was obtained by the radiolytic oxidation at 77 K of a dilute solution of *anti*-**TOD** in F-113 (*cf.* Figure 1). The sequential photoreactions from a) to b) and b) to c) were carried out with filtered 310–410 nm and 460–580 nm light, respectively, corresponding to regions containing the strong absorption bands of **BOT**$^{\bullet+}$ and **COT**$^{\bullet+}$centered at 395 and 505 nm, respectively. The weak signals of **BOD**$^{\bullet+}$ present in the wings of spectrum b) probably result from the incomplete avoidance of the consecutive photoreactions in the first step. The spectra were recorded with identical spectrometer settings.

Since **COT**$^{\bullet+}$ absorbs strongly in this region with the peak of its EA band at 505 nm, there can be little doubt concerning its correct identification as the photoprecursor of *syn*-**BOD**$^{\bullet+}$ in this experiment. The weak signals from *syn*-**BOD**$^{\bullet+}$ present in

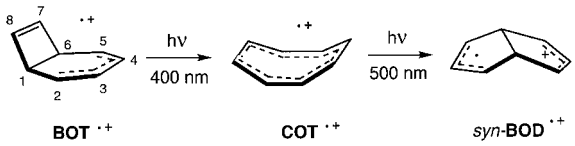

Figure 2b) probably arise from some secondary photoconversion of **COT**$^{\bullet+}$ with the 310–410 nm light rather than directly from **BOT**$^{\bullet+}$. This sequence of reactions represents a "chemical reinforcement" of our assignment of the spectra in Figure 1 to **BOT**$^{\bullet+}$ and thus the observation that *anti*-**TOD**$^{\bullet+}$ undergoes spontaneous ring opening to **BOT**$^{\bullet+}$ on ionization. Table 1 summarizes the experimental and calculated hfc parameters for the above hydrocarbon radical cations.

Table 1. Experimental and calculated hyperfine couplings of C_8H_8 radical cations.

Radical cation	Source of hf data	Hyperfine couplings [G]		
BOT$^{\bullet+}$	expt[a]	25.8(2H)	7.5 (4H)	3.8(2H)
	calc[b]	24.1($H_{1,6}$)	−9.0($H_{2,5}$) 7.0($H_{7,8}$)	3.2($H_{3,4}$)
COT$^{\bullet+}$	expt	Not resolved ca. 10 G envelope[a]		1.5(8H)[c]
	calc[b]			−2.51(8H)
syn-**BOD**$^{\bullet+}$	expt[a]	36.2(2H)	7.7(4H)	(not resolved)
	calc[b]	36.8($H_{1,5}$)	−8.5($H_{2,4,6,8}$)	2.4($H_{3,7}$)
1,4-**DHP**$^{\bullet+}$	expt[a]	11.9(2H)	(not resolved)	(not resolved)
	calc[b]	−10.8($H_{2,5}$)	0.7($H_{3,6}$)	−0.4(2H_1, 2H_4)

[a] This work; measured in solid chlorofluorocarbon matrices; [b] B3LYP/6–31G*; [c] Measured in solution: R. M. Dessau, *J. Am. Chem. Soc.* **1970**, *92*, 6356.

Ionization of *anti*-TOD by photoinduced electron transfer: Further confirmation of the above finding comes from a chemically induced nuclear spin polarization (CIDNP) experiment (Figure 3) in which *anti*-**TOD** was oxidized by photoinduced electron transfer from triplet chloranil in solution. CIDNP arises because two competing processes which may follow the initial electron transfer (diffusional separation and intersystem crossing to the singlet ion pair, respectively) show a different dependence on the nuclear spin state. This leads to a sorting of nuclear spins in the products and gives rise to NMR signals in enhanced absorption and/or emission.[8] The observed polarization pattern is determined by magnetic parameters of the radical cation (the relative magnitude of its *g*-factor, Δg, and the hyperfine coupling constants of its nuclei, A) and by reaction parameters, such as the initial spin multiplicity of the radical ion pair μ, and the mechanism of product formation ε.[9] Conversely, the CIDNP effects of a polarized product can be used to identify the hyperfine coupling (hfc) pattern of the radical ion intermediate and to determine its electron spin density distribution.

Accordingly, the CIDNP technique has been applied successfully to probe the structures of a range of radical cations.[8, 10, 11] In cases of radical cation rearrangements that take place on timescales of a nanosecond or less, the observed

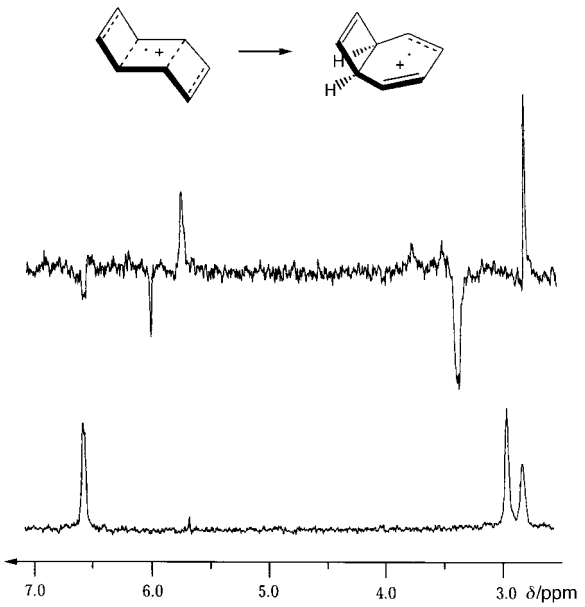

Figure 3. 60 MHz ^{1}H-NMR spectrum in [D_6]acetone containing each 10^{-2} M of *anti*-**TOD**$^{\bullet+}$ and chloranil (bottom), and CIDNP-difference spectrum (4 FIDs recorded during UV irradiation minus 4 FIDs recorded in the dark; top). The allylic emission signal ($\delta = 3.35$) and the olefinic signals, in enhanced absorption ($\delta = 5.6$) and in emission ($\delta = 5.9$) are assigned to $H_{1,6}$, $H_{2,5}$, and $H_{7,8}$, respectively, of **BOT**.

polarization pattern can be strikingly characteristic of the longer-lived secondary radical cation rather than that of the primary radical cation.

Indeed, we found in the present case that irradiation of chloranil in the presence of *anti*-**TOD** fails to generate any polarization for the starting compound; thus, the allylic ($\delta =$ 2.95) and olefinic signals ($\delta = 6.5$) present in the NMR spectrum, obtained in the dark, of *anti*-**TOD**/chloranil (Figure 3, lower) only contribute insignificantly to the CIDNP spectrum (Figure 3, upper).

However, three significantly enhanced signals were observed, a broad allylic emission signal ($\delta = 3.35$) and two olefinic signals, one in enhanced absorption ($\delta = 5.6$), the other one in emission ($\delta = 5.9$; Figure 3, top). The chemical shifts of the three enhanced signals are very close to those reported for **BOT**;[12] accordingly, we assign them to a single polarized product **BOT**. This assignment implies that the primary radical cation *anti*-**TOD**$^{\bullet+}$ has a very short lifetime (< 1 ns) and rearranges rapidly to **BOT**$^{\bullet+}$. The secondary species is kinetically stable; its interaction with the chloranil radical anion generates the observed spin polarization, which is then "trapped" by return electron transfer into the neutral diamagnetic product **BOT**.

Concerning the structure of **BOT**$^{\bullet+}$, the polarization pattern supports negative hfcs (enhanced absorption) for the butadiene fragment (H_{2-5}) and positive hfcs (emission) for the allylic ($H_{1,6}$) and olefinic ^{1}H nuclei of the cyclobutene fragment in the corresponding radical cation. These results support a radical cation in which spin and charge are localized on the carbons of the butadiene fragment; however, the CIDNP experiment cannot distinguish the spin density at $C_{2,5}$ from that at $C_{3,4}$ because the olefinic resonances, $H_{2,5}$ and $H_{3,4}$, are overlapping. Interestingly, both the allylic bridgehead protons ($H_{1,6}$) and the olefinic ^{1}H nuclei of the cyclobutene ring ($H_{7,8}$) show emission; this suggests that both types of nuclei interact with the unpaired electron spin by π,σ-delocalization (hyperconjugation). This type of interaction is unexceptional for the bridgehead β-hydrogens but much less common for the olefinic protons.

Radiolytic oxidation of *anti*-TOD in F-114B2/F-11 and MCH/BuCl: In view of the above-described results, which were not entirely unexpected, we were very surprised to find that γ-irradiation of *anti*-**TOD** in the F-11/F-114B2 Freon mixture, which on cooling to 77 K yields a suitably transparent glass for optical studies, leads to an EA spectrum standing in stark contradiction to that expected for **BOT**$^{\bullet+}$ (Figure 4a). In fact, it shows unmistakably the presence of another C_8H_8 isomer, namely the radical cation of 1,4-dihydropentalene (1,4-**DHP**$^{\bullet+}$) whose authentic EA spectrum has been unambigously assigned before,[6, 7] and which is reproduced for reference purposes (Figure 4c), dashed line).

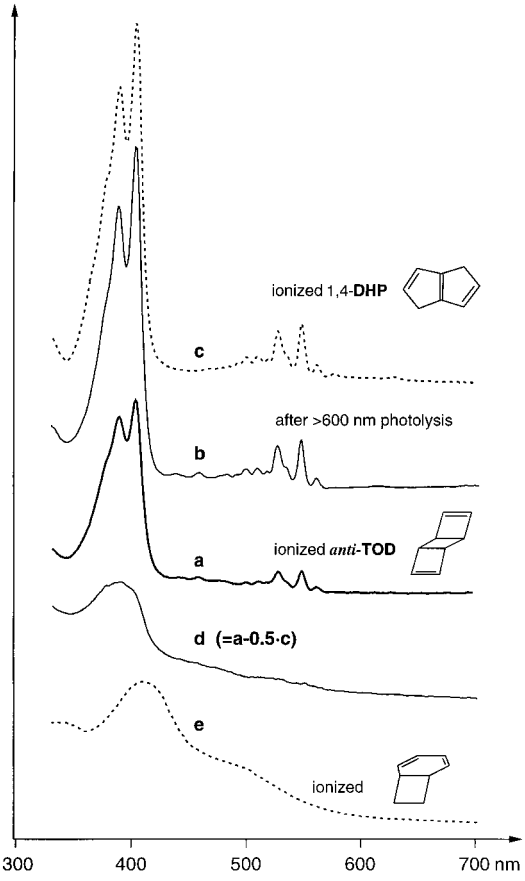

Figure 4. a) Electronic absorption (EA) spectrum obtained after ionization of *anti*-**TOD** in F-114B2/F-11; b) same sample after 30 min photolysis at > 590 nm; c) EA spectrum obtained after ionization of 1,4-**DHP** under the same conditions.[6] Spectrum c) shows the result of a scaled subtraction of b) or c) from a) whereas e) is the spectrum obtained after ionization of bicyclo[4.2.0]octa-2,4-diene.[13]

A similar spectrum was observed after pulse-radiolysis in the MCH/BuCl mixture (Figure 5). This experiment demonstrates also that the observed spectrum arises within microseconds even at 10 K. Thermal relaxation of the matrix (or radiolysis at higher temperature) leads to an increase in the

0947-6539/00/0605-0852 $ 17.50+.50/0 *Chem. Eur. J.* **2000**, *6*, No. 5

1,4-**DHP**$^{\bullet+}$ spectrum. This implies that at 10 K a precursor of 1,4-**DHP**$^{\bullet+}$ is formed and that this precursor rearranges to the

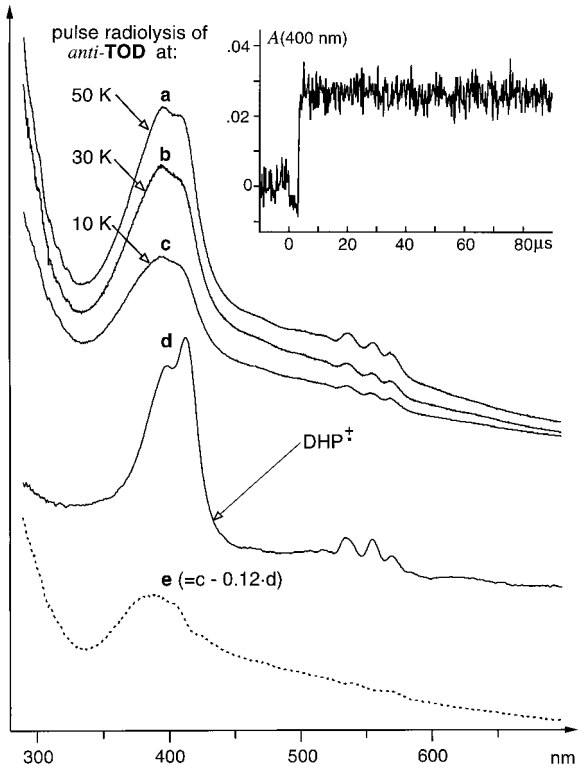

Figure 5. a)–c) EA spectra obtained after pulse radiolysis (25 pulses, dose 25 kGy) of *anti*-**TOD** in MCH/BuCl at the three indicated temperatures, d) EA spectrum of 1,4-**DHP**$^{\bullet+}$ obtained as a secondary photoproduct of **COT**$^{\bullet+}$in MCH/BuCl (10 pulses, dose 10 kGy, 77 K), e) difference spectrum (the weight of spectrum d) was adjusted for optimal cancellation of the **DHP**$^{\bullet+}$ bands around 550 nm). Inset: formation of the 400 nm absorption signal at 10 K (4 μs electron pulse, dose 1 kGy).

dihydropentalene cation at higher temperature. However, as is shown in Figure 4b, this rearrangement is incomplete even at 77 K because another approximately twofold increase of the bands of 1,4-**DHP**$^{\bullet+}$ can be effected by $\lambda > 600$ nm photolysis (the same experiment, not shown, was also done in the hydrocarbon matrices). Hence, ionization of *anti*-**TOD** must give rise, in addition to the products identified above, to a precursor for 1,4-**DHP**$^{\bullet+}$ which a) must absorb above 600 nm, but b) shows only absorptions which are either too weak to be observed or coincide with the increasingly strong bands of 1,4-**DHP**$^{\bullet+}$. The calculations presented in the section on theoretical results and discussion will allow us to propose a hypothesis with regard to the identity of this stealthy species. Note that the spectrum after full conversion is practically identical to that obtained from a sample of ionized authentic 1,4-**DHP**$^{\bullet+}$ (Figure 4c).[6]

Closer examination of the optical spectra obtained in the two experiments reveals, however, some subtle differences with those of 1,4-**DHP**$^{\bullet+}$ obtained in the same media. First, we note that the relative intensities of the peaks in the two vibrational progression of the 400 nm band system are slightly different in spectra a) and b) of Figure 4, and much more distinctly so in Figure 5a)–c), and d). This suggests that the spectra obtained on ionization of *anti*-**TOD** contain, next to 1,4-**DHP**$^{\bullet+}$, a component which absorbs more strongly on the high-energy side of the 400 nm band of 1,4-**DHP**$^{\bullet+}$. Indeed, after subtraction of a suitably scaled authentic spectrum of 1,4-**DHP**$^{\bullet+}$ a similar trace is obtained in both experiments (Figures 4d and 5e) which shows a great similarity to that of ionized bicyclo[4.2.0]octa-2,4-diene,[13] replotted in Figure 4e) for the purpose of comparison.

On the basis of this similarity, and in view of the fact that the ESR and CIDNP experiments described above had clearly revealed the presence of **BOT**$^{\bullet+}$ as a product of ionization of *anti*-**TOD**, we ascribe spectra 4d) and 5e) to **BOT**$^{\bullet+}$. It is, however, important to note that the relative intensities of the bands of 1,4-**DHP**$^{\bullet+}$ and **BOT**$^{\bullet+}$ are *not* proportional to the relative amount of these two species, because their absorptivities differ considerably.

In order to further probe this surprising dependence of the fate of ionized *anti*-**TOD** on the experimental conditions we returned to ESR spectroscopy in F-114B2 which—in contrast to the mixture with F-11 used for optical spectroscopy—allowed us to obtain reasonable spectra of radical cations, albeit at lower resolution than in the other Freons.[6] Figure 6a) shows the spectrum obtained at 151 K after oxidation of *anti*-**TOD** at 77 K in this matrix. On first consideration this looks like a poorly resolved version of the **BOT**$^{\bullet+}$ spectra in Figure 1. However, illuminaton of the sample at 315–395 nm, which

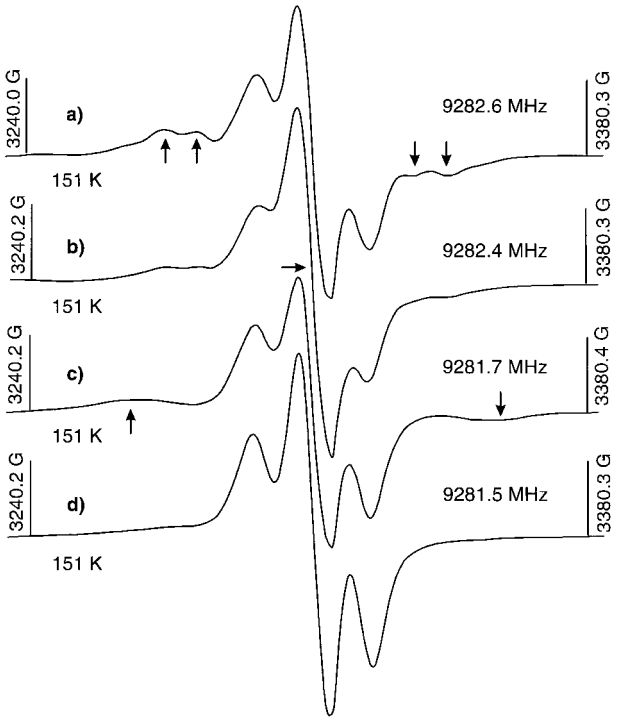

Figure 6. First-derivative ESR spectra recorded at 151 K a) after the radiolytic oxidation at 77 K of a dilute solution of *anti*-**TOD** in CF_2BrCF_2Br, b) after subsequent exposure of the sample to 310–410 nm light, c) after further exposure to 350–580 nm light, and d) after final exposure to red light ($\lambda > 540$ nm). The sequential photo bleaching converts signals from **BOT**$^{\bullet+}$ (double arrows) in a) to those of **COT**$^{\bullet+}$ (horizontal arrow) in b), to those of **BOD**$^{\bullet+}$ (single arrows) in c), and to those of 1,4-**DHP**$^{\bullet+}$ in d). The main signal carrier present initially in a) is 1,4-**DHP**$^{\bullet+}$ as revealed by the prominent triplet features ($a(2\mathrm{H}) = 11.9$ G) which define the final spectrum d) consisting only of 1,4-**DHP**$^{\bullet+}$. The spectra were recorded with identical spectrometer settings.

results in a bleaching of the broad **BOT**$^{\bullet+}$ signals marked with double arrows in spectrum a), does *not* strongly affect the dominant 11.9 G triplet, except for the expected increase of the center line due to the formation of **COT**$^{\bullet+}$ (horizontal arrow, cf. Figure 2b).

The subsequent conversion of **COT**$^{\bullet+}$ to **BOD**$^{\bullet+}$ on 460–580 nm irradiation can also be observed (see broad outermost features marked by single arrows), but once again the central triplet is not changed. Only on exposure to red light ($\lambda >$ 515 nm) which bleaches **BOD**$^{\bullet+}$ does this signal increase by about 30% to give spectrum d) in Figure 6. Actually, this spectrum is identical to that observed previously after oxidation of 1,4-**DHP** in F-114B2.[6] If we assume that all of the **BOT**$^{\bullet+}$ initially present was converted by the series of photolyses described above to 1,4-**DHP**$^{\bullet+}$, we conclude from this experiment that about 70% of the total ESR signal obtained after oxidation of *anti*-**TOD**$^{\bullet+}$ in F-114B2 must be due to 1,4-**DHP**$^{\bullet+}$, in good accord with the results from the optical spectra.

Thus, different experiments led us to the conclusion that on ionization of *anti*-**TOD**, the two valence isomers 1,4-**DHP**$^{\bullet+}$ and **BOT**$^{\bullet+}$ are spontaneously formed in a ratio that seems to depend very strongly on the medium and the way in which the ionization is effected. Obviously, *anti*-**TOD**$^{\bullet+}$ is not stable, even at 10 K under conditions where excess energy is efficiently dissipated, and it engages in two competitive decay pathways whose mechanistic details will be elucidated by quantum chemical calculations in the following section.

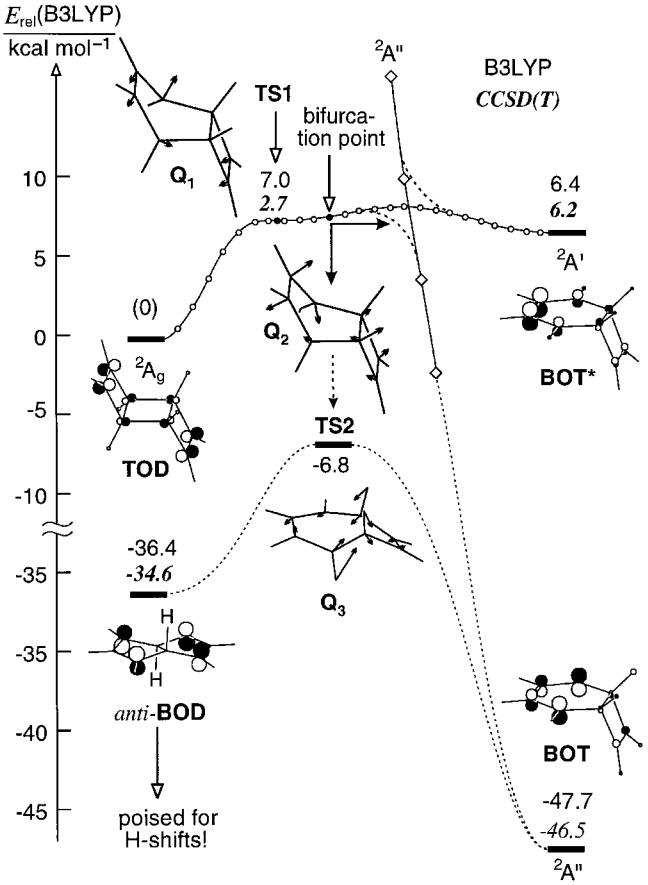

Figure 7. B3LYP/6–31G* potential energy surfaces for the valence isomerization of *anti*-**TOD**$^{\bullet+}$ to **BOT**$^{\bullet+}$ and to *anti*-**BOD**$^{\bullet+}$, respectively. Italic numbers denote CCSD(T)/cc-pVDZ single point energies at B3LYP geometries, corrected for B3LYP zero point energy differences.

Theoretical Results and Discussion

The photoelectron (PE) spectra of *syn*- and *anti*-**TOD** had been investigated and discussed in the mid-1970s[14, 15] in connection with discussions of through-space and through-bond interactions of π-systems.[16–19] Thereby it was established that the ground state of *anti*-**TOD**$^{\bullet+}$ has A_g symmetry, that is, the a_g-MO of *anti*-**TOD** depicted on the left side of Figure 7 is singly occupied (=Somo). In view of the conversion to **BOT**$^{\bullet+}$ this implies that the ground state of *anti*-**TOD**$^{\bullet+}$ correlates with an excited state of **BOT**$^{\bullet+}$ in which an MO of a′ symmetry is singly occupied (in contrast to the ground state, see right side of Figure 7).

According to B3LYP and CCSD(T) calculations, the lowest ^{2}A′ excited state of **BOT**$^{\bullet+}$ lies at slightly higher energy than the ground state of *anti*-**TOD**$^{\bullet+}$, but it is possible to calculate a diabatic reaction path for this interconversion in C_s symmetry (line with open dots in Figure 7). At some point along this pathway, the A″ surface that connects to the ground state of **BOT**$^{\bullet+}$ (line with diamonds) cuts steeply through the A′ surface, and it is to be expected that the system would cross over to that state by loss of symmetry (dashed lines), rather than continue on the way to excited ^{2}A′ **BOT**$^{\bullet+}$.

The first stationary point encountered on this C_s pathway (first filled dot) is a flat saddle point **TS1**, which lies 7 kcal mol^{-1} above *anti*-**TOD**$^{\bullet+}$ by B3LYP but only 2.7 kcal mol^{-1} by CCSD(T). The associated imaginary normal mode $\mathbf{Q_1}$ shows the expected features for the transition state of the *anti*-**TOD**$^{\bullet+}$ → **BOT**$^{\bullet+}$ interconversion. However, instead of leading to a minimum on the far side, proceeding along the C_s reaction coordinate leads to a *bifurcation* or a valley-ridge inflection in the potential energy surface (second filled dot) at almost the same energy as the transition state. This expresses itself in the appearance of a *second* imaginary normal mode $\mathbf{Q_2}$ perpendicular to $\mathbf{Q_1}$ (which represents the *anti*-**TOD**$^{\bullet+}$ → **BOT**$^{\bullet+}$ reaction coordinate). Following this symmetry-breaking mode results in a steep descent which eventually conducted us to a new saddle point **TS2** (associated imaginary normal mode: $\mathbf{Q_3}$) well below *anti*-**TOD**$^{\bullet+}$.

Intrinsic reaction coordinate calculations, whereby the bottom of potential energy valleys leading from saddle points to minima are followed, revealed that **TS2** corresponds to the transition state for the rearrangement of (ground state) **BOT**$^{\bullet+}$ to a new $C_8H_8^{\bullet+}$ species which turns out to be a conformational isomer of *syn*-**BOD**$^{\bullet+}$[3] with the bridgehead hydrogen atoms in an *anti* position. In order to distinguish this from the "normal" *syn*-configured isomer we will call this very strained molecule *anti*-**BOD**$^{\bullet+}$.

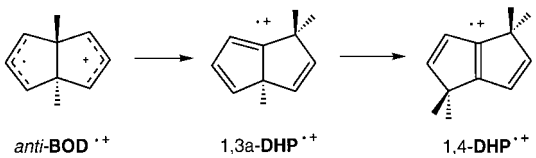

0947-6539/00/0605-0854 $ 17.50+.50/0 *Chem. Eur. J.* **2000**, *6*, No. 5

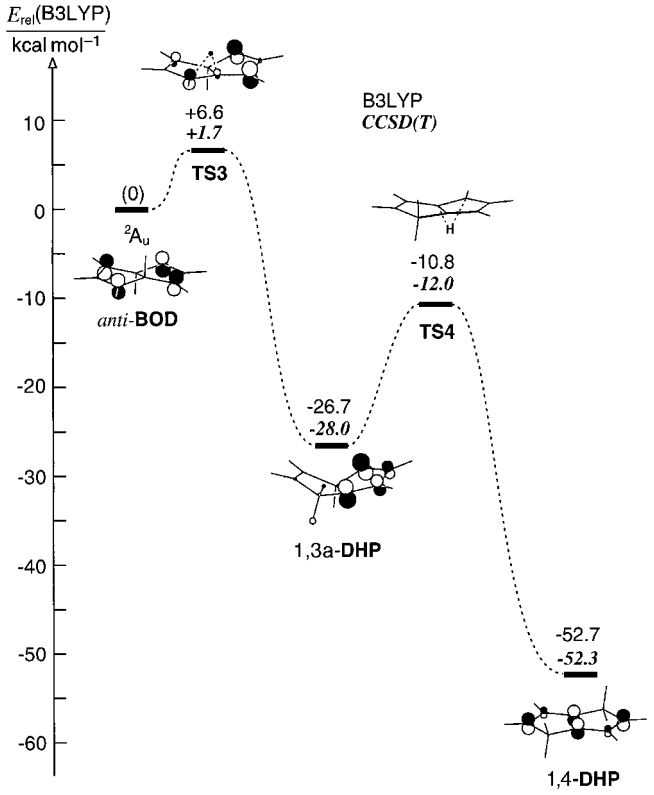

Figure 8. B3LYP/6–31G* potential energy surface for the decay of *anti*-**BOD**$^{\bullet+}$ by successive hydrogen atom shifts to 1,4-**DHP**$^{\bullet+}$. Italic numbers denote CCSD(T)/cc-pVDZ single point energies at B3LYP geometries, corrected for B3LYP zero point energy differences.

Similar to *syn*-**BOD**$^{\bullet+}$,[3, 20] the FMOs of *anti*-**BOD**$^{\bullet+}$ are composed of linear combinations of the antisymmetric allylic π-MOs. However, the ordering of the linear combinations is now reversed in that the *antibonding* combination ($7a_u$, cf. MO depicted on the leftmost side of Figure 8) is singly occupied in the *anti* isomer, in contrast to the *syn* isomer where the SOMO corresponds to the bonding combination. The reason for this is that through-space interaction of the allylic MOs is entirely suppressed owing to the planarization induced by the *anti* configuration of the HCCH bridge. However, the bonding (symmetric) combination is destabilized by interaction with the bridgehead C–H bonds which raises it above the antibonding combination, thus resulting in the "unnatural" sequence of MOs $10a_g(\pi) > 7a_u(\pi)$.

Table 2. Results of CASSCF/CASPT2 calculations for *anti*-**BOD**$^{\bullet+}$.[a]

State	CASSCF/ eV [b]	CASPT2/ eV	(nm)	f[c]
1^2A_u	(0)	(0)		–
1^2A_g	1.07	0.91	(1356)	0.0905
1^2B_u	2.49	2.42	(512)	0[d]
1^2B_g	2.98	2.88	(432)	0.0025
2^2B_g	3.61	3.31	(380)	0.0503
2^2B_u	3.82	3.64	(340)	0[d]
2^2A_g	4.15	4.21	(295)	0.0088
3^2B_g	5.05	4.43	(281)	0.1157
2^2A_u	4.42	4.50	(276)	0[d]

[a] Geometry optimized by B3LYP/6–31G*; ANO-S basis set; [b] active space: 13 electrons in 12 orbitals; details of the calculations are given in the Supporting Information; [c] calculated oscillator strength for electronic transition; [d] dipole-forbidden transition.

According to CASPT2 calculations (see Table 2), the excited state where the a_g π-MO is singly occupied lies less than 1 eV above the ground state.[21] The NIR electronic transition leading to this state is predicted to be so intense that any presence of *anti*-**BOD**$^{\bullet+}$ could not have failed to express itself in the absorption spectra (no bands of important intensity are predicted throughout the visible region). However, careful inspection of the NIR region never revealed any bands in these spectra. Hence, if the pathway suggested by the above calculations is indeed followed, a rapid process must be leading to the loss of *anti*-**BOD**$^{\bullet+}$ in our experiments.

A closer inspection of the geometry and the electronic structure of *anti*-**BOD**$^{\bullet+}$ suggests one such process, namely hydrogen migration: the angle between the bridgehead C–H bond and the C–C bond leading to the allyl moieties (which carry most of the charge) is only 99°, and the dihedral angle to the axis of the terminal allylic p-AOs is only 7°. Thus, it comes as no surprise that the computed activation barrier for H-migration to form the radical cation of 1,3a-dihydropentalene (1,3a-**DHP**$^{\bullet+}$) via **TS3** is very low (1.7 kcal mol^{-1} at the CCSD(T) level). In the course of the reaction, spin and charge separate into opposite allyl moieties (cf. SOMO of **TS3** in Figure 8), which further facilitates the migration of the hydrogen atom to the now nearly vacant "target" p-AO. This explains why the intriguing *anti*-**BOD**$^{\bullet+}$ is probably no more than a fleeting intermediate in the decay of ionized *anti*-**TOD**$^{\bullet+}$.

In contrast, the resulting 1,3a-dihydropentalene radical cation (1,3a-**DHP**$^{\bullet+}$) is protected by a higher barrier (transition state **TS4**) from a second H-shift leading to the final observed product 1,4-**DHP**$^{\bullet+}$ (≈16 kcal mol^{-1} by both B3LYP and CCSD(T)). As 1,3a-**DHP**$^{\bullet+}$ is formed in a nearly activationless, very exothermic process from *anti*-**TOD**$^{\bullet+}$, it would not be surprising if some of the incipient 1,3a-**DHP**$^{\bullet+}$ would have sufficient excess energy to cross **TS4** (which is unsurmountable after thermalization at 77 K). Nevertheless, part of the 1,3a-**DHP**$^{\bullet+}$ will remain trapped in that local minimum, and this may constitute the population that gives rise to more 1,4-**DHP**$^{\bullet+}$ on photolysis at > 600 nm.

In order to examine if this hypothesis is viable, we wanted to compute the electronic absorption spectrum of 1,3a-**DHP**$^{\bullet+}$ by the CASPT2 method, but unfortunately, all attempts to arrive at a consistent and satisfactory description of the excited states above 300 nm by this method failed. Qualitatively, the spectrum of 1,3a-**DHP**$^{\bullet+}$ should be similar to that of the cyclopentadiene radical cation (weak band extending from 480 to 610 nm, strong band at 365 nm),[22] supplemented by a weak transition involving charge transfer from the olefin to the diene moiety in the near IR. Thus, 1,3a-**DHP**$^{\bullet+}$ certainly fulfills one of the conditions for the photoprecursor of 1,4-**DHP**$^{\bullet+}$, that is a weak absorption above 600 nm. If the sharp 365 nm band of cyclopentadiene$^{\bullet+}$ happens to be shifted in 1,3a-**DHP**$^{\bullet+}$ so it coincides with the strong 400 nm peak of 1,4-**DHP**$^{\bullet+}$, its decrease on photolysis would be masked by the increase of the latter. However, it is still surprising that 1,3a-**DHP**$^{\bullet+}$ does not show up in the difference spectrum (Figure 4d), which leaves our hypothesis of this species being the "optically silent" precursor of 1,4-**DHP**$^{\bullet+}$ spectroscopically unconfirmed.[23]

Since previous work has shown that the photoexcited state of *syn*-**BOD**$^{\bullet+}$ is readily converted to 1,4-**DHP**$^{\bullet+}$,[3] the present study provides evidence that the *ground state* of *anti*-**BOD**$^{\bullet+}$, which can be formed from *anti*-**TOD**$^{\bullet+}$ without ring inversion, is similarly predisposed to undergo the hydrogen transfers from the bridgehead carbons. The intermediacy of *anti*-**BOD**$^{\bullet+}$ on the reaction pathway from *anti*-**TOD**$^{\bullet+}$ contrasts with the fact that only *syn*-**BOD**$^{\bullet+}$ is formed from *syn*-**TOD**$^{\bullet+}$, again without ring inversion, and also from photoexcited **COT**$^{\bullet+}$. This finding nicely points up the subtle importance of stereochemical considerations in dictating the course of these rearrangements.

Conclusion

We have shown by different forms of spectroscopy that, upon ionization, *anti*-**TOD** spontaneously decays to more stable products. One of these is the radical cation of bicyclo[4.2.0]octa-2,4,7-triene (**BOT**) which formally arises by electrocyclic opening of one of the cyclobutene rings. **BOT**$^{\bullet+}$ is the predominant product in crystalline Freon matrices at 77 K (ESR) as well as in photoinduced electron transfer from triplet excited chloranil at room temperature (CIDNP). On the other hand, in glassy Freon or hydrocarbon matrices, another rather unexpected product appears very prominently, namely the radical cation of 1,4-dihydropentalene (1,4-**DHP**). This product arises already at 10 K but only becomes predominant at 77 K in Freon glasses.

An investigation of the $C_8H_8^{\bullet+}$ potential energy surface with the B3LYP/6-31G* density functional method reveals a possible mechanism that explains the formation of both products. It involves, shortly after the very low-lying transition state which connects *anti*-**TOD**$^{\bullet+}$ to the first excited state of **BOT**$^{\bullet+}$, a bifurcation on the potential surface which leads to the partitioning between a channel that continues on to **BOT**$^{\bullet+}$, and another one that conducts eventually to a hitherto unknown $C_8H_8^{\bullet+}$ isomer, the *anti* form of the bicyclo[3.3.0]octa-2,6-diene-4,8-diyl radical cation (*anti*-**BOD**$^{\bullet+}$). This latter species is poised to undergo an easy [1,2]-hydrogen shift leading to the radical cation of 1,3a-dihydropentalene (1,3a-**DHP**$^{\bullet+}$) which may in turn decay by a further H-shift to the observed 1,4-**DHP**$^{\bullet+}$. The different quantum chemical results presented in this study are in accord with all observations, including the enigmatic photochemical enrichment of 1,4-**DHP**$^{\bullet+}$ in Freon glasses.

Apparently, the fate of the partially ring-opened *anti*-**TOD**$^{\bullet+}$ on encounter of the bifurcation is strongly dependent on environmental parameters such as the dielectric and mechanical properties of the medium in which it is generated. To our knowledge, this is the first such example of a product partitioning that has been explained in terms of a potential energy bifurcation.

Experimental Section

Synthesis: *anti*-Tricyclo[4.2.0.0^{2,5}]octa-3,7-diene (*anti*-**TOD**) was synthesized by dehalogenation of dichlorocyclobutene[24] (Fluka, purum) by Li amalgam which was prepared in situ according to the procedure of Alexander and Rao.[25] In the workup, the conversion to the silver complex[24] was replaced by purification by preparative gas chromatography at room temperature using β,β'-oxidiproprionitrile (ODP) as a stationary phase.

Sample preparation: $\approx 5 \times 10^{-3}$ M solutions of *anti*-**TOD** were prepared in $CFCl_2CFCl_2$ (F-112), CF_2ClCCl_3 (F-112a), $CF_2ClCFCl_2$ (F-113), CF_3CCl_3 (F-113a) for ESR-measurements, or a 1:1 mixture of $CFCl_3$ (F-11) and CF_2BrCF_2Br (F-114B2),[26, 27] or 1M *n*-butyl chloride (BuCl) in methylcyclohexane (MCH) for optical studies. These solutions were filled into quartz tubes (ESR work) or special optical cuvettes,[28]where they were exposed to $\approx$0.5 MRad of ^{60}Co γ-radiation at 77 K.

Pulse radiolysis: The samples (2 mm thick) were mounted in a liquid helium-cooled cryostat (Oxford Instruments) and irradiated with 4μs electron pulses (delivering a dose $\approx$1 kGy) from ELU-6 linear accelerator. Details of the pulse radiolysis system are given elsewhere.[29]

Spectroscopy: All ESR measurements were carried out on a Bruker ER 200 D SRC spectrometer (TE_{102} cavity, ER-4102-ST X-band resonator, 35 dB microwave power) equipped with variable-temperature accessories. Electronic absorption (EA) spectra were measured on a Perkin–Elmer Lambda 19 (200–2000 nm), a Philips 8710 (200–900 nm) and a Cary 5 (Varian, 200–3300 nm) instrument. CIDNP experiments were carried out by irradiation of the sample in the probe of a Bruker 60 MHz NMR spectrometer equipped with a fused silica light-pipe. The collimated beam of a Hanovia 1000-W high pressure Hg/Xe lamp was passed through a water filter and an aqueous $CuSO_4$ filter solution. A total of four FIDs each were collected during irradiation and in the dark.

Quantum chemical calculations: The geometries of all species were optimized at the UHF and UMP2 level as well as by methods based on density functional theory (DFT). For the latter we used Becke's hybrid 3-parameter (B3) exchange functional[30] which was combined with the Lee–Yang–Parr correlation functional[32] to give the B3-LYP method[33] as implemented in the Gaussian 94 package of programs.[34] The above calculations were all done with the standard 6–31G* basis set. Except where otherwise indicated, stationary points were identified at all levels by Hessian calculations. In addition, transition states were characterized by full intrinsic reaction coordinate (IRC) calculations[35] to identify the minima they interconnect. Finally, single-point calculations were carried out on stationary points (usually at the B3LYP geometries) by the RCCSD(T) method[36] with Dunning's correlation-consistent polarized double-zeta basis set (cc-pVDZ),[37] using the MOLPRO program.[38]

For excited states we resorted to the CASSCF/CASPT2 procedure[39] with the MOLCAS program.[40] The active spaces were chosen such that the weight of the CASSCF wavefunction in the final CASPT2 wavefunction was similar for all states considered (a description of the active spaces for each molecule is given in the footnotes to Tables 1–3; detailed informations on the calculations are given in the Supporting Information). As in previous cases of radical cations,[41–43] satisfactory agreement with experiment was obtained with the simple [C]3s2p1d/[H]2s ANO DZ basis set,[44] and therefore we saw no necessity to add higher angular momentum and/or diffuse functions. Molecular orbitals were plotted with the MOPLOT program,[45] which gives a schematic representation of the MOs nodal structures in a ZDO-type approximation.[46]

Acknowledgment

This work is part of project/grant No. 2000-053568.98 of the Swiss National Science Foundation (Fribourg Group), No. 3T09A 11809 of the Polish State Committe for Scientific Research, and grant No. CHE-9714840 of the US National Science Foundation (Rutgers Group). The research of the Knoxville Group was supported by the Division of Chemical Sciences, Office of Basic Energy Sciences, U.S. Department of Energy, under Grant No. DE-FG02-88ER13852. In addition H.R. acknowledges financial support through the NSF equipment grant CHE-9520633.

[1] K. Hassenrück, H.-D. Martin, R. Walsh, *Chem. Rev.* **1989**, *89*, 1125.
[2] S. Dai, J. T. Wang, F. Williams, *J. Am. Chem. Soc.* **1990**, *112*, 2837.
[3] T. Bally, L. Truttmann, S. Dai, F. Williams, *J. Am. Chem. Soc.* **1995**, *117*, 7916.

0947-6539/00/0605-0856 $ 17.50+.50/0 *Chem. Eur. J.* **2000**, *6*, No. 5

[4] R. Gleiter, *Top. Curr. Chem.* **1979**, *86*, 197.
[5] S. Dai, J. T. Wang, F. Williams, *J. Am. Chem. Soc.* **1990**, *112*, 2835.
[6] T. Bally, L. Truttmann, S. Dai, J. T. Wang, F. Williams, *Chem. Phys. Lett.* **1993**, *212*, 141.
[7] T. Bally, L. Truttmann, J. T. Wang, F. Williams, *J. Am. Chem. Soc.* **1995**, *117*, 7923.
[8] See e. g.: H. D. Roth, *Top. Curr. Chem.* **1992**, *163*, 131.
[9] a) G. L. Closs, *Adv. Magn. Reson.* **1974**, *7*, 157; b) R. Kaptein, *Adv. Free Radical Chem.* **1975**, *5*, 319; c) J. H. Freed, J. B. Pederson, *Adv. Magn. Reson.* **1976**, *8*, 2; d) F. J. Adrian, *Rev. Chem. Intermed.* **1979**, *3*, 3.
[10] a) H. D. Roth, M. L. M. Schilling, *J. Am. Chem. Soc.* **1980**, *102*, 7956; b) H. D. Roth, M. L. M. Schilling, *J. Am. Chem. Soc.* **1981**, *103*, 1246.
[11] a) H. D. Roth, T. Herbertz, *J. Am. Chem. Soc.* **1993**, *115*, 9804; b) H. D. Roth, T. Herbertz, *J. Am. Chem. Soc.* **1997**, *119*, 9574.
[12] E. Vogel, H. Kiefer, W. R. Roth, *Angew. Chem.* **1964**, *76*, 432; *Angew. Chem. Int. Ed. Engl.* **1964**, *3*, 442.
[13] T. Bally, K. Roth, R. Straub, *Helv. Chim. Acta* **1989**, *72*, 73.
[14] R. Gleiter, E. Heilbronner, M. Hekman, H. D. Martin, *Chem. Ber.* **1973**, *106*, 28.
[15] H.-D. Martin, S. Kagabu, R. Schwesinger, *Chem. Ber.* **1974**, *107*, 3130.
[16] R. Hoffmann, A. Imamura, W. J. Hehre, *J. Am. Chem. Soc.* **1968**, *90*, 1499.
[17] R. Hoffmann, *Acc. Chem. Res.* **1971**, *4*, 1.
[18] R. Hoffmann, E. Heilbronner, R. Gleiter, *J. Am. Chem. Soc.* **1970**, *92*, 706.
[19] R. Gleiter, *Angew. Chem.* **1974**, *86*, 770; *Angew. Chem. Int. Ed. Engl.* **1974**, *13*, 696.
[20] T. Bally, L. Truttmann, F. Williams, *J. Mol. Struct. (Theochem)* **1997**, *398*, 255.
[21] Loss of the C_{2h} symmetry plane would allow this state to mix with the ground state, and this vibronic interaction may lead to a spontaneous distortion of *anti*-**BOD**$^{\bullet+}$ to C_2 symmetry which entails a localization of the spin in one and charge in the other allyl moiety. In *syn*-**BOD**$^{\bullet+}$ the corresponding energy gain was offset by the loss of the stabilizing through-space interaction between the two allylic moieties.[20] However, in the *anti* conformer, such interaction is virtually absent, and hence it cannot oppose a localization of spin and charge. In fact, re-optimization of *anti*-**BOD**$^{\bullet+}$ in C_2 symmetry at noncorrelated levels leads to a substantial energy decrease (9.9 kcal mol^{-1} by UHF, 6.9 kcal mol^{-1} by ROHF, 8.9 kcal mol^{-1} by CASSCF(5,6)). In contrast, B3LYP geometry optimizations converge invariably to a C_{2h} equilibrium structure (the C_2 structures lying 2–3 kcal mol^{-1} higher in energy), but this may be due to the reluctance of DFT methods to overstabilize inherently symmetric radical ions possessing delocalized spin and charge.[31] However, single point calculations at the C_{2h} and C_2 CASSCF geometries by the CCSD(T) method predict an energy increase of 6 kcal mol^{-1} on distortion and hence the preference for the higher symmetry appears to be a dynamic correlation effect.
[22] L. Truttmann, K. R. Asmis, T. Bally, *J. Phys. Chem.* **1995**, *99*, 17844.
[23] A reviewer has suggested the attractive possibility of a concerted double hydrogen atom transfer to explain the direct formation of 1,4-**DHP**$^{\bullet+}$ from *anti*-**TOD**$^{\bullet+}$, arguing that, if a single H-shift has such a low barrier that for a double shift cannot be so much higher. While this is probably true, the barrier for a single H-shift will undoubtedly remain lower, so this process will invariably "win". Also the barrier for a concerted double H-shift may be substantially higher because the migrating H-atoms can only profit half as much from the localization of charge on the terminal allylic centers as in the case of the single H-shift. While we cannot exclude that some of the 1,4-**DHP**$^{\bullet+}$ is indeed formed directly by double H-shift, this pathway certainly does not represent the lowest energy one.
[24] M. Avram, I. G. Dinulescu, E. Marcia, G. Meteescu, E. Sliam, C. D. Nenitzescu, *Chem. Ber.* **1964**, *97*, 382.
[25] J. Alexander, G. S. K. Rao, *J. Chem. Educ.* **1970**, *47*, 277.
[26] C. Sandorfy, *Can. J. Spectrosc.* **1965**, *85*, 10.
[27] A. Grimison, G. A. Simpson, *J. Phys. Chem.* **1968**, *72*, 1776.
[28] T. Bally in *Radical Ionic Systems* (Eds.: A. Lund, M. Shiotani), Kluwer, Dordrecht, **1991**, pp. 3–54.
[29] S. Karolczak, K. Hodyr, R. Lubis, J. Kroh, *Radioanal. Nucl. Chem.* **1986**, *101*, 177.
[30] A. D. Becke, *J. Chem. Phys.* **1993**, *98*, 5648.
[31] T. Bally, G. N. Sastry, *J. Phys. Chem. A* **1997**, *101*, 7923.
[32] C. Lee, W. Yang, R. G. Parr, *Phys. Rev. B* **1988**, *37*, 785.
[33] B. G. Johnson, P. M. W. Gill, J. A. Pople, *J. Chem. Phys.* **1993**, *98*, 5612.
[34] M. J. Frisch, G. W. Trucks, H. B. Schlegel, P. M. W. Gill, B. G. Johnson, M. A. Robb, J. R. Cheeseman, T. Keith, G. A. Petersson, J. A. Montogomery, K. Raghavachari, M. A. Al-Laham, V. G. Zakrzewski, J. V. Ortiz, J. B. Foresman, J. Cioslowski, B. B. Stefanov, A. Nanayakkara, M. Challacombe, C. Y. Peng, P. Y. Ayala, W. Chen, M. W. Wong, J. L. Andres, E. S. Repogle, R. Gomperts, R. L. Martin, D. J. Fox, J. S. Binkley, D. J. DeFrees, J. Baker, J. P. Stewart, M. Head-Gordon, M. C. Gonzales, J. A. Pople, Gaussian, Inc., Pittsburgh, PA, **1995**.
[35] C. Gonzales, H. B. Schlegel, *J. Chem. Phys.* **1989**, *90*, 2154.
[36] Coupled-cluster method with single and double excitations supplemented by a non-iterative estimation of the contributions of triple excitations, based on a spin-restricted HF zero-order wavefunction. P. J. Knowles, C. Hampel, H.-J. Werner, *J. Chem. Phys.* **1993**, *99*, 5219.
[37] D. E. Woon, T. H. Dunning, *J. Chem. Phys.* **1993**, *98*, 1358.
[38] J.-J. Werner, P. J. Knowles, J. Almlöf, R. D. Amos, M. J. O. Deegan, S. T. Elbert, C. Hampel, W. Meyer, K. Peterson, R. Pitzer, A. J. Stone, P. R. Taylor, R. Lindh, MOLPRO 96, **1996**.
[39] K. Andersson, B. O. Roos in *Modern Electronic Structure Theory*, *Part 1*, *Vol. 2*, World Scientific Publ., Singapore, **1995**, pp. 55.
[40] K. Andersson, M. R. A. Blomberg, M. P. Fülscher, V. Kellö, R. Lindh, P.-Å. Malmqvist, J. Noga, J. Olson, B. O. Roos, A. Sadlej, P. E. M. Siegbahn, M. Urban, P.-O. Widmark, MOLCAS 4, University of Lund, Sweden, **1994**.
[41] M. P. Fülscher, S. Matzinger, T. Bally, *Chem. Phys. Lett.* **1995**, *236*, 167.
[42] Z. Zhu, T. Bally, J. Wirz, M. Fülscher, *J. Chem. Soc. Perkin Trans. 2* **1998**, 1083.
[43] T. Bally, C. Carra, M. P. Fülscher, Z. Zhu, *J. Chem. Soc. Perkin Trans. 2* **1998**, 1759.
[44] P.-O. Widmark, P.-Å. Malmqvist, B. O. Roos, *Theor. Chim. Acta* **1990**, *77*, 291.
[45] T. Bally, B. Albrecht, S. Matzinger, M. G. Sastry, MOPLOT 3.2, University of Fribourg **1997**.
[46] E. Haselbach, A. Schmelzer, *Helv. Chim. Acta* **1979**, *54*, 1299.

Received: May 22, 1999 [F1875]